Enhanced 4-chlorophenol adsorption from aqueous solution using eco-friendly nanocomposite

Fadia A. Sulaiman[1] , Rasha Khalid Sabri Mhemid[2*] , Noor A. Mohammed[3]

[1] Department of Geomatics Techniques Engineering, College of Technical Engineering, Mosul, Northern Technical University, 41001 Mosul, Iraq
[2] Department of Environmental Technologies, College of Environmental Sciences, University of Mosul, 41001 Mosul, Iraq
[3] Department of Environmental Engineering, University of Baghdad, 10071 Baghdad, Iraq
* Corresponding author's email: rashamhemid@uomosul.edu.iq

ABSTRACT

Adsorption of 4-chlorophenol (4-CP) via magnetite/SiO_2/xanthan were investigated using batch scale experiments. The study aims to prepare a green nanocomposite (NC) and determine whether it is effective in removing 4-CP. To synthesize NC (magnetite/SiO_2/xanthan) from Alocasia macrorrhiza extract, a simple, and green method was applied. X-ray diffraction (XRD), Fourier-transform infrared spectroscopy (FTIR), and scanning electron microscopy (SEM) were used to identify the prepared NC. The response surface modeling (RSM) was employed to optimize operational variables in the adsorption process of 4-chlorophenol (4-CP) from an aqueous solution using NCs as an adsorbent. The results indicate that the oxidation percentage of 4-CP is 89.47%, at ideal conditions [temperature (25 °C), 4-CP concentration (10 mg/L), contact time (180 minutes), rpm speed (200), pH (3), and adsorbent dose (1 g/L)]. Moreover, the model's normal reaction results have a sensible likeness to the actual data (R^2 = 95.19), exhibiting the productivity of this technique in making an exact forecast. A second-order polynomial multiple regression model was utilized to assess the responses, which affirms that it was a satisfactory adjustment (R^2 = 0.9864) with the accomplished data through investigation of variance (R^2 = 95.19%, R^2 adj = 94.34% and R^2 pred = 93.24%).

Keywords: 4-chlorophenol, adsorption, green synthesis, nanocomposite, alocasia macrorrhiza, magnetite, response surface method.

INTRODUCTION

Chlorophenols (CPs) are organic substances that are released into the environment by a variety of processes. It is well known that CPs are highly toxic and they can seriously damage the ecosystem and human health as well. The United States Environmental Protection Agency (EPA) confirmed these compounds are potentially toxic materials (Kralik et al., 2010). The European Community published a poison list that included numerous CPs, laying out their maximum allowable concentration in drinking water of (0.5 g/L) for these chemicals (Mustafa & Shihab, 2013). As a result of several human activities,

e.g. water treatment, waste incineration, pesticides and herbicides used uncontrollably, and by-products of chlorine bleaching, these chemicals are introduced into the environment (Pera-Titus et al., 2004). CPs possess bactericidal properties that increase with chlorination. The phytotoxicity of CPs is highly sensitive to plants. In the case of aquatic organisms, CPs are absorbed through the gills, intestines, or skin of fish. In the present study, 4-chlorophenol (4-CP) was used as a model pollutant. Symptoms of acute (4-CP) health effects may occur immediately or shortly following exposure. In case of skin or eye contact (irritant), it can be extremely hazardous (Pérez-Portuondo et al., 2021). It is possible to lose vision or

damage the cornea as a result of eye contact. Inflammation and blistering can occur as a result of skin contact. It can cause lung damage, choking, unconsciousness, or even death in severe cases of overexposure (De & Leyva, 2017). The substance might be poisonous to the liver, mind, gastrointestinal plot, upper respiratory lot, and peripheral nervous system (Czaplicka, 2004). The toxicity of CPs and the difficulty of removing them from the environment makes them hazardous to the environment, especially since they have little biodegradability and are difficult to remove (Zada et al., 2021). As a result of low biodegradability and as common wastewater treatment technologies are insufficiently effective in removing it. Therefore, modern techniques were used to remove these pollutants such as adsorption technology.

There are several advantages to the adsorption process, starting with its high efficacy, reasonable cost, ease of design and operation and easy-to-use process that treats wastewater and makes it recyclable. The advantage of adsorption is that it produces no toxic end products (Alwared et al., 2023; Hao et al., 2015). Adsorption strategies were generally used to wipe out organic chemical compounds in dirtied destinations utilizing suitable adsorbent (Homem & Santos, 2011). A few change strategies, such as nanotechnology methods, have been recommended to improve the adsorption capability of pesticides used in farming. Nanotechnology is viewed as one of the intriguing advancements, the development of nanosized, usable designs (1–100 nm) (Shafqat et al., 2023). Recent research has focused on using nanoparticles to remove contaminants. These properties provide enhanced efficiency and cost-effectiveness, which are driving their interest. Nanoparticles are highly effective in this application due to their high surface area and abundance of active sites (Akter et al., 2012).

In this study, nanomaterials were prepared from nanoparticles and xanthan gum to eliminate 4-chlorophenol (4-CP). A straightforward, eco-accommodating, and green technique was utilized to synthesize magnetite/SiO_2/xanthan (NCs), which the Fe_2O_3 was extracted from the Alocasia macrorrhiza plant. Elephant's ear, a member of the Araceae family, is widely used for decorative purposes, its aesthetic appeal, and various medical purposes. The authors (He et al., 2016) detailed that Alocasia macrorrhiza contains a few phytochemicals including succinic corrosive, flavonoids, glycosides, ascorbic corrosive, fructose, amino acids, beta-sitosterol, stigmasterol, sucrose, campesterol, citrus

extract, malic corrosive, alocasia, and glucose. Due to the presence of several antioxidant constituents (vitamins and flavonoids) in this plant, it was selected as a bioreducer and stabilizing agent in this study (Ali et al., 2020). This nanocomposite (NCs) was also synthesized using xanthan gum, an anionic heteropolysaccharide produced by the bacterium Xanthomonas campestris. Xanthan gum has garnered significant attention from researchers due to its practical applications and its nature as a natural polymer. It is widely used in various industries for its unique properties (Jadav et al., 2023). When polymer (Xanthan gum) is added to aqueous solutions, it increases viscosity due to inter- and intramolecular forces within the polymer and between the polymer and the surrounding molecules (Camesano & Wilkinson, 2001). Besides the NCs used in this work, SiO_2 was also used to enhance its properties, particularly its ability to exchange cations easily and its small size (Abu Elella et al., 2021). A surface interaction between NP-SiO_2 and xanthan chain functional groups results in the polymer chains joining the ($^-$OH/H) groups of NP-SiO_2. A recent study has suggested that NP-SiO_2 limits xanthan conformational transitions (Kennedy et al., 2015). NP-SiO_2 and polymer interact in nanofluids to create new cross-linked structures. This process improves xanthan gum (XG) solutions by delaying conformational transitions (Pi et al., 2016).
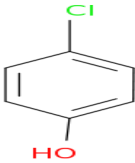
The goal of this work is to study the effectiveness of 4-CP adsorption as one of the main compounds of the CPs. The adsorbent material chosen for this study was a greenly synthesized magnetite/SiO_2/xanthan nanocomposite. Different variables were selected throughout the treatment to accomplish the experimental goals: 4-CP concentration, pH, contact time, NCs dose, and shaking speed. The removal efficiency was optimized using response surface modeling (RSM).

MATERIALS AND METHODS

Materials

Table 1 provides some information about 4-CP. Among the chemicals purchased from the Merck company with a purity higher than 99 % were iron (III) chloride ($FeCl_3$), sodium metasilicate (Na_2SiO_3), methanol, n-hexane, ethanol and xanthan gum. By adding HCl or NaOH to the solution, the pH was adjusted.

Table 1. Physical and chemical properties of 4-chlorophenol (Bilgili et al., 2012)

Property	4-Chlorophenol
Chemical structure	
Formula	ClC_6H_4OH
Density (318 K)	1.26 g/cm³
Molecular weight	128.56 g/mol
Solubility in water (293 K)	27 g/L
Surface area	$3.26 \times 10{-}19$ m²/gm
pKa	9.41

Synthesis of magnetite/SiO$_2$/xanthan nanocomposite

To prepare the extract, 50 grams of powdered leaves of the Alocasia macrorrhiza plant were boiled in 400 mL of double-distilled water for 40 minutes at 80 °C. A 250-mL beaker was filled with 100 mL of the filtered extract and 2 g of $FeCl_3$ and 5 g of Na_2SiO_3, at 80 °C and pH 10. The solution was filtered after a black precipitate was formed. After stopping stirring, the solution was filtered so that the precipitate could be separated. To ensure full oxidation of each nano fraction, the precipitate was heated to 400 °C and washed with hot distilled water to remove impurities. Additionally, 15 g of xanthan gum was added to 200 mL of ethanol and refluxed for 8 hours at 80 °C, resulting in the precipitation of a magnetite/SiO$_2$/xanthan nanocomposite, which was magnetically separated (Ali et al., 2020). A scanning electron microscope (SEM) was used to characterize Fe_3O_4/mineral-soil nanocomposite. Fourier-transform infrared spectroscopy (FTIR) and X-ray diffraction (XRD) were used to analyze the mineralogical composition of the nanomaterials. As a result of the Brunauer-Emmett-Teller (BET) method, the specific surface area of the nanocomposite was determined, and the total pore volume was estimated from the nitrogen adsorbed at a relative pressure of about 0.99. The zeta potential of the nanocomposite was measured using a ZETASIZER Nano-ZS90 (Malvern, UK) (Shihab et al., 2024). A detailed description of the synthesizing steps for the mentioned NCs can be found in Figure 1.

Batch adsorption studies

4-CP aqueous solution was investigated for adsorption using a thermostatic orbital shaker (Rivotek, Kolkata, India) as shown in Figure 2 Several experimental parameters were adjusted to determine the optimal adsorption conditions, including solution pH, temperature, contact time, agitation speed, and initial 4-CP concentration. Double-distilled deionized water was used to prepare a 1000 mg/L stock solution of 4-CP. An adsorbent solution of known concentration was mixed with 50 mL of 4-CP solution. At predetermined intervals, the samples were removed from the shaker, and the 4-CP solution was centrifuged under 10,000 rpm for 10 minutes (REMI Centrifuge, Model: R-24). The solution was analyzed using a UV-Vis spectrophotometer (Shimadzu, Japan, Model: UV 1800) at 225 nm, the wavelength
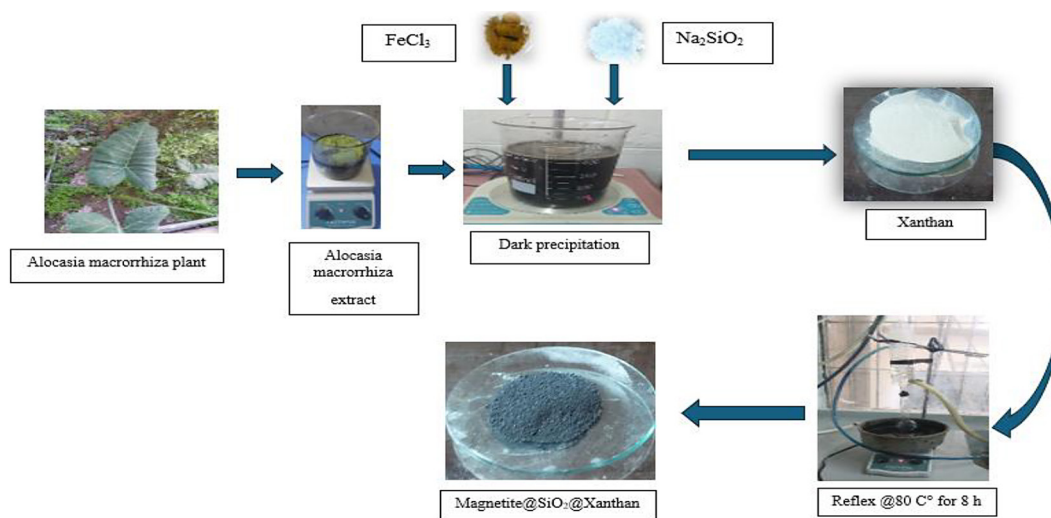

Figure 1. Schematic diagram of the synthesis process for preparing green magnetite/ SiO$_2$/ Xanthan NCs

Figure 2. Shaking device with water path

of maximum 4-CP absorbance. Equation 1 was used to calculate the percentage of 4-CP removal (Majlesi & Hashempour, 2017).

$$CP\ removal\ efficiency = \frac{C_o - C}{C_o} \times 100 \quad (1)$$

where: C_o is the initial 4-CP concentration (mg/L); C_e is the equilibrium 4-CP concentration (mg/L).

RESULTS AND DISCUSSIONS

Characterization of the adsorbent

Fourier-transform infrared spectroscopy

An effective technique for identifying specific functional groups in molecules is Fourier-transform infrared spectroscopy (FTIR). This technique provides insights into the structure of a sample by acquiring an infrared absorption or emission spectrum. In the electromagnetic spectrum, infrared radiation (IR) falls between visible light and microwaves (Salim et al., 2024). The FTIR spectra in the range of 4000–400 cm^{-1} are shown in Figure 3. A FTIR analysis of the nanocomposite confirms the presence of phytochemicals on its surface. OH, functional groups and Fe-O vibrations of Fe_3O_4 molecules are represented by prominent peaks at 3439.42 cm^{-1} and 1646.91 cm^{-1}, respectively. As a result of antisymmetric stretching vibrations between Si-O-Si, the band observed at 1069 cm^{-1} indicates silicon dioxide in the synthesized adsorbent (Peng et al., 2014a). The bending vibration absorption peaks of Si-O-Si and Si-OH were measured at 460.80
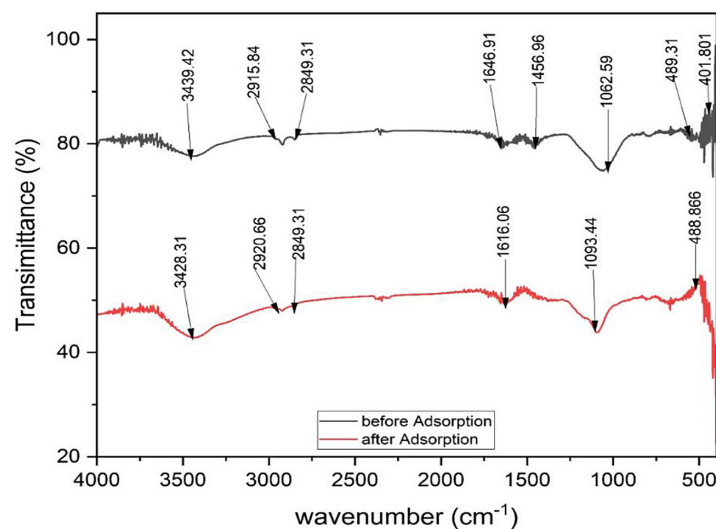

Figure 3. FTIR analysis for magnetite/ SiO$_2$/ xanthan nanocomposites

cm^{-1} and 489.83 cm^{-1}, respectively (Xu et al., 2013). These referred to the existence of silica layer. The antisymmetric and symmetric C-H stretching vibrations observed at 2915.84 cm^{-1} and 2849.31 cm^{-1}, respectively (Sobhanardakani et al., 2018b). The disappearance or emergence of new peaks indicates the interaction between the adsorbent and the pollutant, which indicates a crossover in their chemical bonding or structural characteristics (Sulaiman & Alwared, 2022a).

Scanning electron microscopy

The scanning electron microscopy (SEM) images illustrate the structure of the synthesized adsorbent. In Figure 4a can be shown, the Fe_2O_3 granules have a continuous nanocluster shape that appears as vertical columns. By oxidizing Fe to Fe_2O_3, Fe_2O_3 particles form by diffusing Fe atoms along grain boundaries, which results in the formation of Fe_2O_3 nanoclusters along grain boundaries. Fe_2O_3 nanoclusters interact with one another during the nucleation process, which results in larger clusters being formed (Sobhanardakani et al., 2018a). A certain size and growth time are required for these nanoclusters to become thermodynamically stable (Ingler & Khan, 2004; Kleiman-Shwarsctein et al., 2010). Figure 4b shows the morphology of the synthesized nanocomposite after adsorption. The surface morphology was investigated to gain more insight into the size, shape, morphology, and agglomeration of the green-synthesized magnetite /SiO₂/xanthan nanocomposites (NCs). The results reveal that the homogeneous green NCs exhibit some clustering with a semi-spherical morphology, with sizes ranging from 49 to 78 nm. These findings, supported by the analytical techniques, conclusively demonstrate the successful formation of the green-synthesized magnetite/SiO₂/xanthan NCs. Magnetite/SiO$_2$/xanthan nanocomposites had a BET surface area of 745.8 m^2/g and a total pore volume of 0.5 cm^3/g, respectively. The small size and porous structure of SiO_2 particles are responsible for this effect. The bigger surface region and pore volume give a more prominent number of dynamic locales on a superficial level for additional adsorption of responsive particles, which brings about an adsorption response with higher productivity (Sulaiman & Alwared, 2022c).

X-ray diffraction technique (XRD)

The XRD pattern was collected in the range of 10° to 75°. Figure 5 indicates the cubic phase of Fe_3O_4 is represented by the following diffraction angles: 220, 400, 422, 511, and 440, respectively, confirming the presence of pure Fe_3O_4. A diffraction angle of approximately 23° is also attributed to the silica structure, which is consistent with (Peng et al., 2014b). In order to determine the size of the crystallites in magnetite/ SiO$_2$/xanthan, the Debye-Scherrer formula Equation 2 was applied (Mhemid et al., 2022). According to Match software, the average crystal size was 26.388 nm based on XRD patterns matched against a reference database.

$$D = \frac{K\lambda}{\beta cos\theta} \tag{2}$$

where: D is the mean size of the crystal domains in angstroms, K is Scherrer's constant (0.94), λ is the wavelength of the X-ray radiation (Cu-Kα, 0.15406 nm), β is the full width at half maximum (FWHM) of the diffraction peak after subtracting the instrumental broadening (in radians), and θ is the diffraction angle.
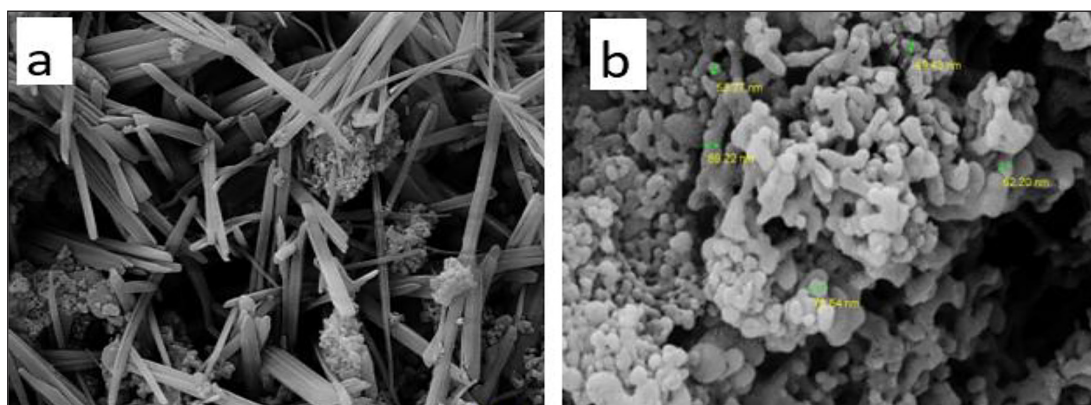

Figure 4. SEM morphologies of the green synthesized magnetite/SiO$_2$/xanthan NCs: (a) before adsorbent, (b) after adsorbent
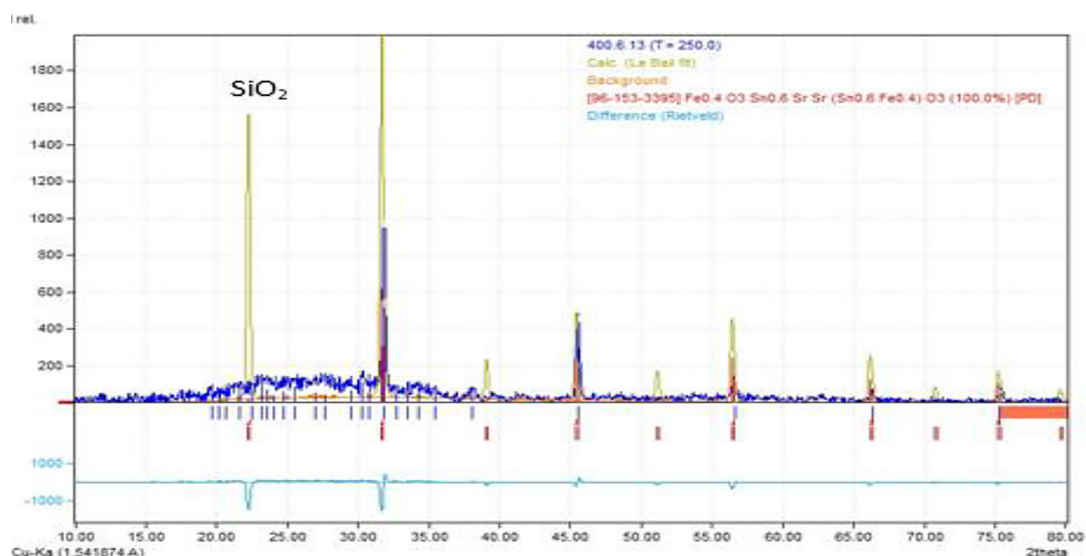
Figure 5. XRD patterns of magnetite/SiO$_2$/xanthan nanocomposites

Adsorption procedure

In batch mode, adsorption experiments were carried out. A variety of factors influence the adsorption of chlorophenols, including the concentration of 4-CP, contact time, shaking speed rpm, pH value, and the adsorbent dose. If these parameters are taken into account, an industrial-scale chlorophenol removal process can be developed. Below, we discuss factors affecting chlorophenol adsorption using response surface methodology (RSM).

RSM analysis

An experimental run is created with the DOE software. As the most commonly used method in DOE, the central composite design (CCD) was chosen in this study. CCD was used to study the effects of 4-CP concentration, magnetite/SiO$_2$/xanthan dosage, agitation speed, temperature, pH, and contact time. A list of variables and their ranges is shown in Table 2, as determined by linking scientific literature and obtaining experimental data using the 4-CP in a preliminary study. Following the whole face-centered CCD experimental plan as a guide, the variables were analyzed at (lowest) and (highest). To model adsorption reactors, RSM was used to create multiple regression equations. The main and interaction effects of all conceivable factor combinations have been calculated. The experimental data were fit to Equation 3 using a second order polynomial for the formulation of regression equations relevant to the oxidation process (Salam et al., 2015)

$$Y = B_0 + B_1X_1 + B_2X_2 + B_3X_3 + B_{11}X_{12} + \\ + B_{22}X_{22} + B_{33}X_{32} + B_{12}X_1X_2 + \\ + B_{23}X_2X_3 + B_{13}X_1X_3 \qquad (3)$$

where: Y means for expected response, xi and xj represent coded variables, Bo; offset term, Bi, Bj, and Bij refer to first-order, quadratic, and interaction effects, and i and j for factor index numbers, respectively.

Based on the probabilistic estimation of error (P) value, model parameters are selected or ignored depending on the confidence level of 0.95. The results produced by CCD were analyzed using analysis of variance (ANOVA). An

Table 2. Experimental range and levels of the independent variables

Factor	Name	Unit	Lower limit	Upper limit	Lower weight	Upper weight	Importance
A	Initial concentration of 4-CP	mg/L	10	50	1	1	3
B	Adsorbent dose	g/L	0.5	2	1	1	3
C	pH		3	11	1	1	3
D	Temperature	C^0	10	40	1	1	3
E	Agitation speed	rpm	100	300			
F	Time	min	15	180	1	1	3

experimental design was created using design expert software, and the interaction effects of independent parameters on response were optimized.

Optimization representation

CCD was used to appraise the percentage of 4-CP removed from aqueous solution based on the results of the experiments (Figure 6 and Table 3). A regression model was developed using RSM's historical data design that suggested fitting the corrosion rate data with a fifth order polynomial model (Majlesi & Hashempour, 2017b). Obtaining the final empirical model based on actual factors, as shown in equation 4, the model was manually reduced and simplified by eliminating irrelevant elements.

$$
\begin{aligned}
4CP\ removal &= -94.38077 - \\
&- (0.330437 \cdot A) + (50.984 \cdot B) + \\
&+ (6.268 \cdot C) + (2.49958 \cdot D) + \\
&+ (0.522825 \cdot E) + (0.646639 \cdot F) - \\
&- (22.355 \cdot B^2) - (0.296146 \cdot C^2) - \\
&- (0.049268 \cdot D^2) - (0.001396 \cdot E^2) - \\
&- (0.00168 \cdot F^2)
\end{aligned} \quad (4)
$$

According to Figure 6, the actual and predicted removal percentages of 4-CP are given. According to the results, this scheme shows reasonable correlations between the points. Regarding the equation addressed here, as the 4-CP concentration was increased, the removal gradually decreased with increasing units of contact time, and as the adsorbent dose was increased, the removal increased, and the model correctly explained the range of experiments tested.

Variance analysis

Analyzing the significance and validity of the model was carried out with ANOVA (Mohammed et al., 2023). The results obtained from the ANOVA analysis (Table 4) illustrated that R^2, adjusted R^2 (R^2_{adj}) and predicted R^2 (R^2_{pred}) for the adsorption of 4-CP were 0.9519, 0.9434 and 0.9324, respectively. Based on the close correlation coefficients, the regression model explains the relationship between the independent variables and the response well. Model terms were evaluated for relevance using their P-values and F-values. In this study, a higher F-value and a lower probability indicated greater relevance for the associated model. The term's significance for the model was determined by its probability value (0.0001) (Mohammed et al., 2024), as shown in Table 5. According to Table 4 the Adeq precision ratio was 34.055%, which refers to an adequate signal. Ideally, Adeq precision should have a ratio of 4 between signal and noise, which is the ratio that determines the accuracy of a signal (Sulaiman & Alwared, 2022b).

Response surface and contour plots

The results were represented using the model-predicted response's 3D response surface and 2D contour plots. As each parameter was varied, the other parameters were kept constant (4-CP concentration, contact time, shaking speed, solution pH, and adsorbent dose) to observe their interaction influence on the response (4-CP removal).

Effect of solution pH

The pH level of the solution influences the adsorbent's capacity to remove chlorophenols from wastewater. The chlorophenol removal capacity of adsorbents depends on the pH of the solution. Because a changing pH of the solution
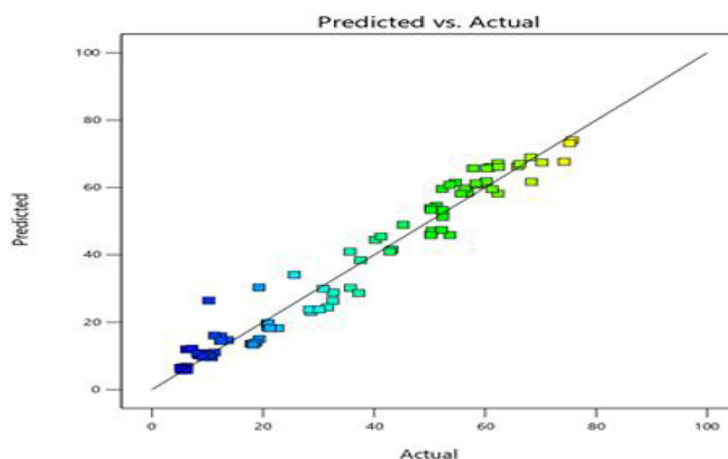

Figure 6. Relation between predicted and actual data of 4-CP removal

Table 3. Results of experiments according to CCD

Run	A: 4-CPconc.	B: Adsorbent dose	C: pH	D: Temperature	E: agitation speed	F: Time	Actual RE %	Prediction RE %
1	30	1	3	25	200	5	24.09	23.03
2	30	1	3	25	200	10	27.19	26.13
3	30	1	3	25	200	15	30.22	29.16
4	30	1	3	25	200	30	38.78	37.72
5	30	1	3	25	200	60	53.65	52.58
6	30	1	3	25	200	90	65.49	64.42
7	30	1	3	25	200	120	74.30	73.23
8	30	1	3	25	200	180	82.86	81.79
9	10	1	3	25	200	5	30.70	14.68
10	10	1	3	25	200	10	33.80	17.79
11	10	1	3	25	200	15	36.83	20.81
12	10	1	3	25	200	30	45.39	29.38
13	10	1	3	25	200	60	60.25	44.24
14	10	1	3	25	200	90	72.09	56.08
15	10	1	3	25	200	120	80.91	74.89
16	10	1	3	25	200	180	89.47	83.44
17	50	1	3	25	200	5	17.48	13.34
18	50	1	3	25	200	10	20.59	15.45
19	50	1	3	25	200	15	23.61	20.47
20	50	1	3	25	200	30	32.17	25.04
21	50	1	3	25	200	60	47.04	35.90
22	50	1	3	25	200	90	58.88	47.74
23	50	1	3	25	200	120	67.69	66.55
24	50	1	3	25	200	180	76.25	75.10
25	30	0.5	3	25	200	5	15.36	12.99
26	30	0.5	3	25	200	10	18.47	16.10
27	30	0.5	3	25	200	15	21.49	19.12
28	30	0.5	3	25	200	30	30.06	27.68
29	30	0.5	3	25	200	60	44.92	42.55
30	30	0.5	3	25	200	90	56.76	54.38
31	30	0.5	3	25	200	120	65.57	63.20
32	30	0.5	3	25	200	180	74.13	71.75
33	30	2	3	25	200	5	8.01	10.90
34	30	2	3	25	200	10	11.11	14.01
35	30	2	3	25	200	15	14.14	17.03
36	30	2	3	25	200	30	22.70	25.59
37	30	2	3	25	200	60	37.57	40.46
38	30	2	3	25	200	90	49.40	52.29
39	30	2	3	25	200	120	58.22	61.11
40	30	2	3	25	200	180	66.78	69.66
41	30	2	7	25	200	5	21.23	13.36
42	30	2	7	25	200	10	24.34	16.47
43	30	2	7	25	200	15	27.36	19.49
44	30	2	7	25	200	30	35.93	28.06
45	30	2	7	25	200	60	50.79	42.92
46	30	2	7	25	200	90	62.63	54.76

47	30	2	7	25	200	120	71.45	63.57
48	30	2	7	25	200	180	80.00	72.12
49	30	2	10	25	200	5	24.93	26.11
50	30	2	10	25	200	10	28.04	29.22
51	30	2	10	25	200	15	31.06	34.24
52	30	2	10	25	200	30	39.63	42.81
53	30	2	10	25	200	60	54.49	55.67
54	30	2	10	25	200	90	66.33	67.51
55	30	2	10	25	200	120	75.15	72.32
56	30	2	10	25	200	180	83.70	74.87
57	30	1	3	10	200	5	12.46	12.88
58	30	1	3	10	200	10	15.57	15.98
59	30	1	3	10	200	15	18.59	19.01
60	30	1	3	10	200	30	27.15	27.57
61	30	1	3	10	200	60	42.02	42.43
62	30	1	3	10	200	90	53.86	54.27
63	30	1	3	10	200	120	62.67	63.08
64	30	1	3	10	200	180	71.23	71.64
65	30	1	3	40	200	5	13.54	11.89
66	30	1	3	40	200	10	16.65	15.00
67	30	1	3	40	200	15	19.67	18.02
68	30	1	3	40	200	30	28.24	26.59
69	30	1	3	40	200	60	43.10	41.45
70	30	1	3	40	200	90	54.94	53.29
71	30	1	3	40	200	120	63.76	62.10
72	30	1	3	40	200	180	72.32	70.65
73	30	1	3	25	100	5	13.68	13.07
74	30	1	3	25	100	10	16.79	16.18
75	30	1	3	25	100	15	19.81	19.20
76	30	1	3	25	100	30	28.38	27.77
77	30	1	3	25	100	60	43.24	42.63
78	30	1	3	25	100	90	55.08	54.47
79	30	1	3	25	100	120	63.90	63.28
80	30	1	3	25	100	180	72.46	71.83
81	30	1	3	25	300	5	6.57	5.94
82	30	1	3	25	300	10	9.68	9.05
83	30	1	3	25	300	15	12.70	12.07
84	30	1	3	25	300	30	21.27	20.64
85	30	1	3	25	300	60	36.13	35.50
86	30	1	3	25	300	90	47.97	47.34
87	30	1	3	25	300	120	56.78	56.15
88	30	1	3	25	300	180	65.34	64.70

leads to differences in ionization levels and surface properties of the adsorptive molecules, the efficiency of adsorption is determined by the pH of the solution. Figure 7 explains the influence of solution pH on chlorophenol adsorption. All the compiled results showed that low pH (acidic) solutions favor chlorophenol adsorption. This is because phenols remain undissociated at lower pH levels, making them more easily absorbed by various adsorbents (Caqueret et al., 2008); (García-Araya et al., 2003). As pH increases, hydroxyl and carboxyl groups dissociate, resulting

Table 4. The results of the analysis of variance for the response quadratic models

Std. Dev	Mean	C.V.	R^2	R^2_{adj}	R^2_{pred}	Adeq precision
5.58	42.58	15.56	0.9519	0.9434	0.9324	34.055

Table 5. The ANOVA results for the design expert software equation

Source	Sum of squares	df	Mean square	F-value	p-value	Comment
Model	44995.93	13	3461.23	111.20	< 0.0001	significant
A-C. of(4-CP)	406.74	1	406.74	13.07	0.0005	
B-Dose of NC	0.1395	1	0.1395	0.0045	0.9468	
C-pH	90.03	1	90.03	2.89	0.0932	
D-Temp.	133.69	1	133.69	4.30	0.0418	
E-Shaking speed	94.33	1	94.33	3.03	0.0859	
F-Time	21282.11	1	21282.11	683.74	< 0.0001	
AF	209.45	1	209.45	6.73	0.0115	
A^2	2078.62	1	2078.62	66.78	< 0.0001	
B^2	1251.31	1	1251.31	40.20	< 0.0001	
C^2	87.89	1	87.89	2.82	0.0972	
D^2	1572.66	1	1572.66	50.53	< 0.0001	
E^2	1778.40	1	1778.40	57.14	< 0.0001	
F^2	5575.02	1	5575.02	179.11	< 0.0001	
Residual	2272.21	73	31.13			
Cor Total	47268.14	86				

in a decrease in adsorption (Raja et al., 2005). A significant increase in the adsorptive removal of 4-CP on magnetite /SiO_2/xanthan nanocomposites was observed as the pH decreased from 10 to 3, reaching its extreme at pH 3.0. However, after increasing the initial pH values from 3 to 10, the adsorption amount of 4-CP was decreased (Yang et al., 2017), found that an acidic pH was better for the adsorption process and that both chlorophenol removal percentages diminished as the pH of the solution increased. Generally, chlorophenol removals decreased with an increase in pH due to them being proton donor (Garba & Rahim, 2016). According to (Hamad et al., 2010), chlorophenols are converted to anions at a certain pH (when the liquid pH overdoes their dissociation constant (pKa) that reduces the adsorption due to the repulsive force between the phenoxide ions and the negative groups on the surface by increasing the negative charge of phenoxide ions. A chemical characteristic of the adsorbents, usually magnetite/SiO_2/xanthan with an acidic point of zero charge (pHpzc), would also explain why the total surface charge is positive at pHpzc higher than the solution pH, but negative at pHpzc lower than the solution pH. Because chlorophenols dissociate when the pH of the solution is high (basic), the percentage of chlorophenol removal decreases. A negative charge on the adsorbent surface produces electrostatic repulsion between it and the chlorophenolate anions in the solution. Furthermore, chlorophenols and OH ions may compete for ion exchange, resulting in reduced removal efficiency (Garba et al., 2019).

Influence of adsorbents dose

Determining the ideal dose is crucial for enhancing the elimination process. It has been observed that a slight increase in the dose of magnetite/SiO_2/xanthan, at a fixed initial 4-CP concentration, leads to an increase in adsorption capacity, as shown in Figure 8. This improvement is due to the obtainability of more adsorption locations and a larger adsorbent surface area resulting from the higher dose. The binding rate of phenolic compounds with adsorbents is more rapid in the original stages but slows down as adsorption reaches a marginal level and eventually decreases. Consequently, the optimal adsorbent dosage was measured to be 1 g/L for 10 mg/L of 4-CP (Ghaffari et al., 2014).
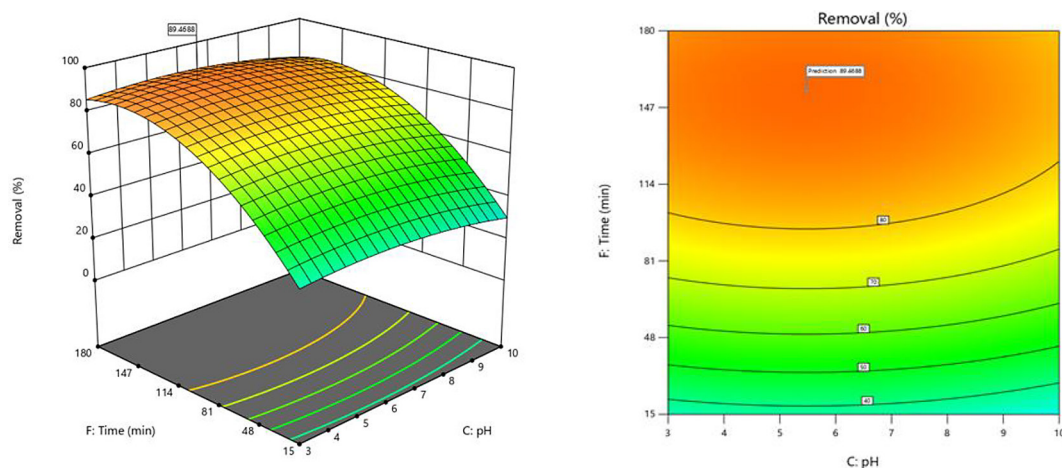
Figure 7. Contour plots express and 3D surface plot of pH on removal efficiency at 4-CP concentration 10 mg/l, dose of adsorbent 1 g/l, agitation speed 200 rpm, contact time 180 min and temperature 25 °C
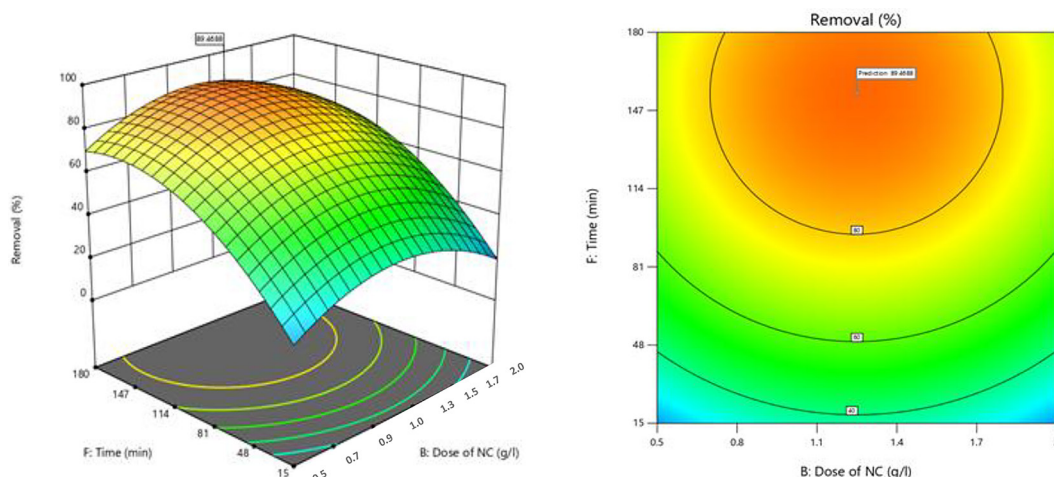

Figure 8. Contour plots express and 3D surface plot of adsorbents on removal efficiency at 4-CP concentration 10 mg/l, PH 3, agitation speed 200 rpm, contact time 180 min and temperature 25 °C

Effect of initial chlorophenol concentration and contact time

Chlorophenol adsorption is significantly affected by the initial concentration of pollutant and the contact time. As shown in Figure 9, initial concentration has a significant effect on 4-chlorophenols adsorption. Chlorophenols are generally removed rapidly at first, followed by a gradual decline until equilibrium is reached (Ren et al., 2011a). Because there are many vacant active sites on the adsorbent, the gradient of concentration between the solution and the adsorbate is higher in the initial stage. Over time, the repulsive forces between solute molecules make filling the remaining vacant sites more difficult (Sobhanardakani et al., 2018c; Ren et al., 2011b; Tan et al., 2009a). Saturation of the

adsorbent and a reduced number of available active sites are responsible for the decrease in adsorption momentum over time (Anoop Krishnan et al., 2011a). Dynamic equilibrium occurs when negligible adsorption is observed at the end of the adsorption process. The equilibrium between adsorption and desorption was reached on the adsorbent surface at this point. Chlorophenols were first affected by the boundary layer effect, which affected their movement. Following diffusion, they adsorb at the adsorbent surface. This allowed the chlorophenols to diffuse deeper into the porous structure of the adsorbent, resulting in a deeper adsorption. This sequence of events illustrates the key stages of the adsorption mechanism, including external diffusion, surface adsorption, and internal diffusion into the pores of the adsorbent (Tan et al., 2009b).
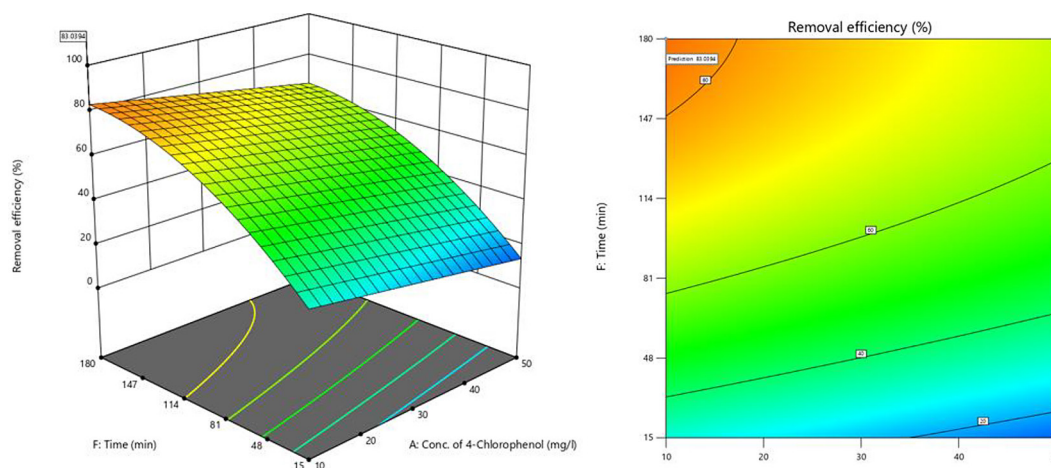
Figure 9. Contour plots express and 3D surface plot of 4-CP concentration on removal efficiency at dose of adsorbent 1 g/l,PH 3 and agitation speed 200 rp

Effect of temperature

In adsorption studies, temperature plays an important role in determining an adsorbent's adsorption capacity. Magnetite/SiO$_2$/xanthan adsorbs chlorophenols with different temperature effects as shown in Figure 10. Exothermic or endothermic processes can occur. Endothermic processes increase adsorption with increasing temperature. With increasing temperatures, there are more active sites available for adsorption because of the increased mobility of the adsorbate molecules (Yagub et al., 2014). At 25 °C result in increased adsorption due to the removal of repulsive forces that act as barriers to adsorption. As the temperature rises, these forces are reduced, making the adsorption process easier (Olu-Owolabi et al., 2017). Due to a decrease in solution viscosity, increasing

the temperature also enhances the surface activity of chlorophenol molecules and their diffusion across the external boundary layer and into the internal pores of adsorbent particles (Agarry et al., 2013). At elevated temperatures, the chlorophenol molecules can also diffuse into the pores of the adsorbent, resulting in an improvement in adsorption capacity (Karthikeyan et al., 2005).

However, a decrease in adsorption capacity was observed above 25 °C. This reduction in adsorption amount might be owing to the weakening of adsorption forces between the adsorbent kind and the active sites on the adsorbent surface caused by an extreme increase in temperature (Yagub et al., 2014).

Effect of agitation speed

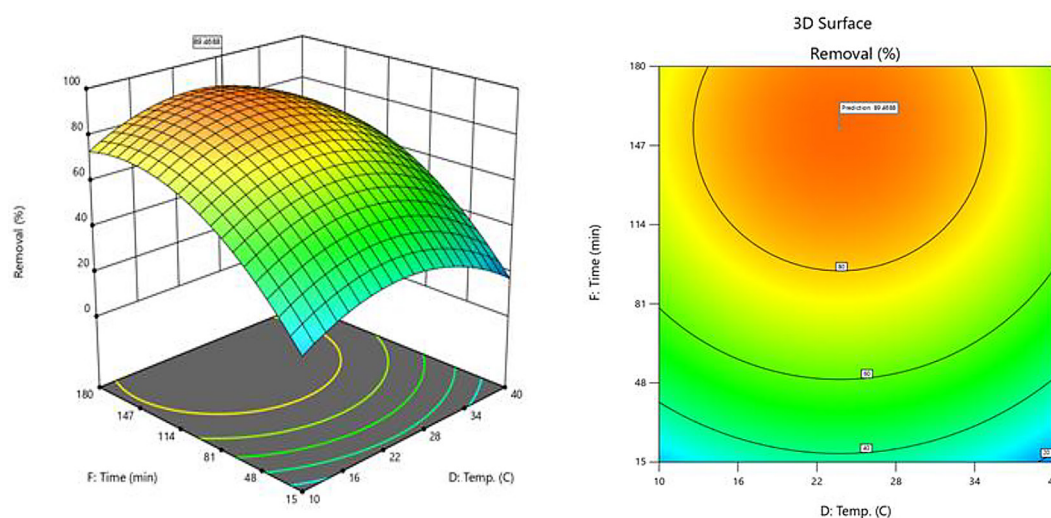The adsorption of 4-CP onto magnetite/SiO$_2$/xanthan was studied as a function of agitation

Figure 10. Contour plots express and 3D surface plot of temperature on removal efficiency at 4-CP concentration 10 mg/l, dose of adsorbent 1 g/l, agitation speed 200 rpm and contact time 180 min

speed at pH 3 over a contact time of 180 minutes. The selected agitation speeds were 100, 200, and 300 rpm, with an initial 4-CP concentration of 10 mg/L. Figure 11 shows that the amount of 4-CP adsorption increases with agitation speed up to 200 rpm, beyond which only a minimal increase in adsorption is observed. The increase in agitation speed promotes proper interaction between 4-CP in the solution and the adsorption sites on magnetite/SiO$_2$/xanthan, enhancing the effective transfer of 4-CP molecules to the adsorbent surface. At 200 rpm, the maximum number of solute-site interactions is achieved, and further increases in agitation speed do not significantly affect adsorption. Therefore, an optimal agitation speed of 200 rpm was chosen for batch adsorption experiments (Krishnan et al., 2011b).

Process optimization

To maximize the removal of 4-CP from an aqueous solution, optimal values were determined for the independent parameters such as 4-CP concentration, magnetite/SiO$_2$/xanthan dosage, agitation speed, temperature, pH, and contact time. A desirability function was created by combining these goals, serving as an objective function with a value of one at the target and zero outside the acceptable range. The program optimizes this function by exploring ways to enhance it. The goal-finding process begins at a random point and advances along the steepest gradient to reach the highest peak (Shihab et al., 2024; Ghorbani & Kamari, 2016). Figure 12 presents the desirability profile of the projected response, indicating the optimal conditions for the independent variables: 4-CP concentration of 25.2857 mg/L, magnetite/SiO$_2$/xanthan dosage of 1.24842 g/L, agitation speed of 193.287 rpm, temperature of 23.7356 °C, pH of 5.47471, and contact time of 154.099 minutes. Under these conditions, the predicted removal efficiency was 83.44%, which closely aligns with the experimentally observed value of 89.47%.
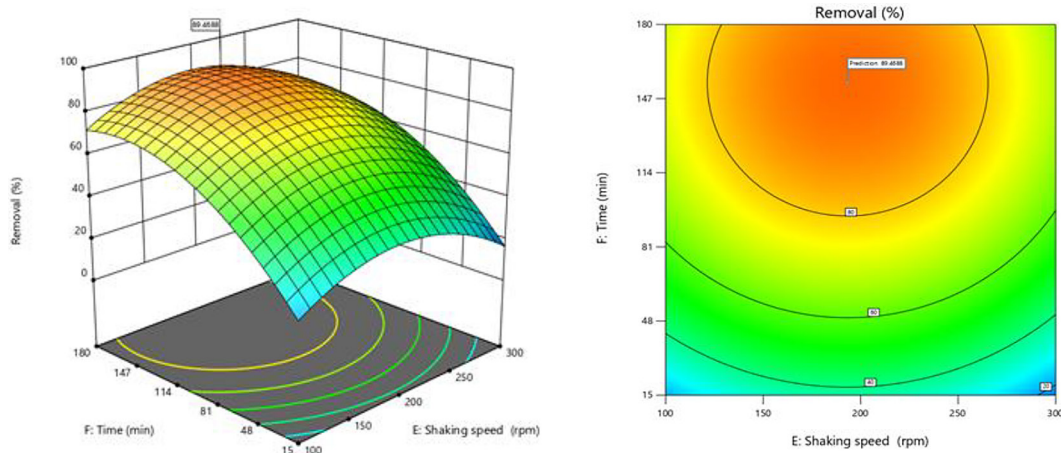

Figure 11. Contour plots express and 3D surface plot of agitation speed on removal efficiency at 4-CP concentration 10 mg/l, dose of adsorbent 1 g/l and contact time 180 min
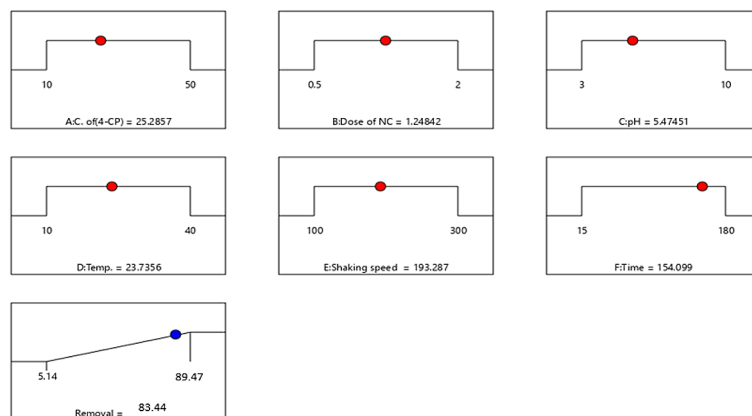

Figure 12. The desirability chart of the estimated response

CONCLUSIONS

In general, magnetite/SiO$_2$/xanthan was highly efficient in removing 4-CP. Synthesizing magnetite/SiO$_2$/xanthan nanoparticles also makes it eco-friendly, stable under various environmental conditions, has low application cost, and produces high volumes. Using an external magnetic field, this adsorbent can easily be removed from water or wastewater.

RSM was applied to optimize the effect of experimental factors on the efficiency of 4-CP removal in the present study, using magnetite/SiO$_2$/xanthan. Based on experimental results, the 2nd order polynomial equation is used to construct an empirical relationship between the response and independent variables. 4-CP was removed with 89.47 percent efficiency at optimum conditions of temperature (25 °C), 4-CP concentration (10 mg/L), contact time (180 minutes), rpm speed (200), pH (3), and adsorbent dose (1 g/L).

ANOVA indicated that the second regression model could be adjusted well to the experimental data (R^2 = 95.19, R^{2}adj = 94.34%, and R^{2}pred = 93.24%). Additionally, 4-CP appears to be adsorption follows pseudo-second order kinetics, with its rate constant being inversely proportional to its initial concentration.

In light of magnetite/SiO$_2$/xanthan magnetic nanocomposite's high efficiency in adsorbing 4-CP, as well as its relatively simple synthesis, it can be used as a suitable adsorbent for organic pollutants removal and degradation.

Acknowledgements

REFERENCES

1. Abu Elella, M. H., Goda, E. S., Gamal, H., El-Bahy, S. M., Nour, M. A., & Yoon, K. R. (2021). Green antimicrobial adsorbent containing grafted xanthan gum/SiO$_2$ nanocomposites for malachite green dye. *International Journal of Biological Macromolecules*, *191*, 385–395. https://doi.org/https://doi.org/10.1016/j.ijbiomac.2021.09.040

2. Agarry, S. E., Owabor, C. N., & Ajani, A. O. (2013). Modified plantain peel as cellulose-based low-cost adsorbent for the removal of 2,6-Dichlorophenol from aqueous solution: adsorption isotherms, kinetic modeling, and thermodynamic studies. *Chemical Engineering Communications*, *200*(8), 1121–1147. https://doi.org/10.1080/00986445.2012.740534

3. Akter, S., Das, P. R., Islam, M. T., Kabir, M. H., Haque, M. M., Khatun, Z., Nurunnabi, M., Khatun, Z., Lee, Y. K., Jahan, R., & Rahmatullah, M. (2012). A selection of medicinal plants used as blood purifiers by folk medicinal practitioners of Bangladesh. *American-Eurasian Journal of Sustainable Agriculture*, *6*(3), 188–194.

4. Ali, J., Manshad, A. K., Imani, I., Sajadi, S. M., & Keshavarz, A. (2020). Greenly synthesized magnetite/SiO$_2$/xanthan nanocomposites and its application in enhanced oil recovery: IFT reduction and wettability alteration. *Arabian Journal for Science and Engineering*, *45*(9), 7751–7761. https://doi.org/10.1007/s13369-020-04377-x

5. Alwared, A. I., Sulaiman, F. A., Raad, H., Al-Musawi, T. J., & Mohammed, N. A. (2023). Ability of FeNi$_3$/SiO$_2$/TiO$_2$ nanocomposite to degrade amoxicillin in wastewater samples in solar light-driven processes. *South African Journal of Botany*, *153*, 195–202. https://doi.org/10.1016/j.sajb.2022.12.031

6. Anoop Krishnan, K., Sreejalekshmi, K. G., & Baiju, R. S. (2011). Nickel(II) adsorption onto biomass based activated carbon obtained from sugarcane bagasse pith. *Bioresource Technology*, *102*(22), 10239–10247. https://doi.org/10.1016/j.biortech.2011.08.069

7. Bilgili, M. S., Varank, G., Sekman, E., Top, S., Özçimen, D., & Yazıcı, R. (2012). Modeling 4-chlorophenol removal from aqueous solutions by granular activated carbon. *Environmental Modeling and Assessment*, *17*(3), 289–300. https://doi.org/10.1007/s10666-011-9293-z

8. Camesano, T. A., & Wilkinson, K. J. (2001). *Single Molecule Study of Xanthan Conformation Using Atomic Force Microscopy*. 1184–1191.

9. Caqueret, V., Bostyn, S., Cagnon, B., & Fauduet, H. (2008). Purification of sugar beet vinasse - Adsorption of polyphenolic and dark colored compounds on different commercial activated carbons. *Bioresource Technology*, *99*(13), 5814–5821. https://doi.org/10.1016/j.biortech.2007.10.009

10. Czaplicka, M. (2004). Sources and transformations of chlorophenols in the natural environment. *Science of the Total Environment*, *322*(1–3), 21–39. https://doi.org/10.1016/j.scitotenv.2003.09.015

11. De, R. F. G., & Leyva, E. (2017). Typha latifolia as potential phytoremediator of 2,4-dichlorophenol: Analysis of tolerance, uptake and possible transformation processes. *ECSN*. https://doi.org/10.1016/j.chemosphere.2016.12.043

12. Garba, Z. N., & Rahim, A. A. (2016). Evaluation of optimal activated carbon from an agricultural waste

for the removal of para-chlorophenol and 2,4-dichlorophenol. *Process Safety and Environmental Protection* 102. Institution of Chemical Engineers. https://doi.org/10.1016/j.psep.2016.02.006

13. Garba, Z. N., Zhou, W., Lawan, I., Xiao, W., Zhang, M., Wang, L., Chen, L., & Yuan, Z. (2019). An overview of chlorophenols as contaminants and their removal from wastewater by adsorption: A review. *Journal of Environmental Management*, *241*(April), 59–75. https://doi.org/10.1016/j.jenvman.2019.04.004

14. García-Araya, J. F., Beltrán, F. J., Álvarez, P., & Masa, F. J. (2003). Activated carbon adsorption of some phenolic compounds present in agroindustrial wastewater. *Adsorption*, *9*(2), 107–115. https://doi.org/10.1023/A:1024228708675

15. Ghaffari, A., Tehrani, M. S., Husain, S. W., Anbia, M., & Azar, P. A. (2014). Adsorption of chlorophenols from aqueous solution over amino-modified ordered nanoporous silica materials. *Journal of Nanostructure in Chemistry*, *4*(3), 1–10. https://doi.org/10.1007/s40097-014-0114-1

16. Ghorbani, F., & Kamari, S. (2016). *Application of response surface methodology for optimization of methyl orange adsorption by Fe-grafting sugar beet bagasse*. https://doi.org/10.1177/0263617416675625

17. Hamad, B. K., Noor, A. M., Afida, A. R., & Mohd Asri, M. N. (2010). High removal of 4-chloroguaiacol by high surface area of oil palm shell-activated carbon activated with NaOH from aqueous solution. *Desalination*, *257*(1–3), 1–7. https://doi.org/10.1016/j.desal.2010.03.007

18. Hao, L., Zheng, T., Jiang, J., Hu, Q., Li, X., & Wang, P. (2015). Removal of As(III) from water using modified jute fibres as a hybrid adsorbent. *RSC Advances*, *5*(14), 10723–10732. https://doi.org/10.1039/c4ra11901k

19. He, Y., Sutton, N. B., Rijnaarts, H. H. H., & Langenhoff, A. A. M. (2016). Degradation of pharmaceuticals in wastewater using immobilized TiO_2 photocatalysis under simulated solar irradiation. *Applied Catalysis B: Environmental*, *182*, 132–141. https://doi.org/10.1016/j.apcatb.2015.09.015

20. Homem, V., & Santos, L. (2011). Degradation and removal methods of antibiotics from aqueous matrices - A review. *Journal of Environmental Management*, *92*(10), 2304–2347. https://doi.org/10.1016/j.jenvman.2011.05.023

21. Ingler, W. B., & Khan, S. U. M. (2004). Photoresponse of spray pyrolytically synthesized magnesium-doped iron (III) oxide (p-Fe_2O_3) thin films under solar simulated light illumination. *Thin Solid Films*, *461*(2), 301–308. https://doi.org/10.1016/j.tsf.2004.01.094

22. Jadav, M., Pooja, D., Adams, D. J., & Kulhari, H. (2023). *Advances in Xanthan Gum-Based Systems for the Delivery of Therapeutic Agents*. 1–27.

23. Karthikeyan, T., Rajgopal, S., & Miranda, L. R. (2005). Chromium(VI) adsorption from aqueous solution by Hevea Brasilinesis sawdust activated carbon. *Journal of Hazardous Materials*, *124*(1–3), 192–199. https://doi.org/10.1016/j.jhazmat.2005.05.003

24. Kennedy, J. R. M., Kent, K. E., & Brown, J. R. (2015). Rheology of dispersions of xanthan gum, locust bean gum and mixed biopolymer gel with silicon dioxide nanoparticles. *Materials Science & Engineering C*, *48*, 347–353. https://doi.org/10.1016/j.msec.2014.12.040

25. Kleiman-Shwarscstein, A., Huda, M. N., Walsh, A., Yan, Y., Stuckyst, G. D., Hu, Y. S., Al-Jassim, M. M., & McMland, E. W. (2010). Electrodeposited aluminum-doped α-Fe2O3 photoelectrodes: Experiment and theory. *Chemistry of Materials*, *22*(2), 510–517. https://doi.org/10.1021/cm903135j

26. Kralik, P., Kusic, H., Koprivanac, N., & Loncaric Bozic, A. (2010). Degradation of chlorinated hydrocarbons by UV/H_2O_2: The application of experimental design and kinetic modeling approach. *Chemical Engineering Journal*, *158*(2), 154–166. https://doi.org/10.1016/j.cej.2009.12.023

27. Majlesi, M., & Hashempour, Y. (2017). Removal of 4-chlorophenol from aqueous solution by granular activated carbon/nanoscale zero valent iron based on Response Surface Modeling. *Archives of Environmental Protection*, *43*(4), 13–25. https://doi.org/10.1515/aep-2017-0035

28. Mhemid, R. K. S., Salman, M. S., & Mohammed, N. A. (2022). Comparing the efficiency of N-doped TiO_2 and commercial TiO_2 as photo catalysts for amoxicillin and ciprofloxacin photo-degradation under solar irradiation. *Journal of Environmental Science and Health, Part A*, *57*(9), 813–829. https://doi.org/10.1080/10934529.2022.2117960

29. Mohammed, N. A., Alwared, A. I., Salim, K., & Sulaiman, F. A. (2024). Synthesis, characterization of $FeNi_3$/SiO_2/CuS for enhance solar photocatalytic degradation of atrazine herbicides: Application of RSM. *Results in Surfaces and Interfaces*, *16*(July), 100253. https://doi.org/10.1016/j.rsurfi.2024.100253

30. Mohammed, N. A., Saeed, L. I., Khalid, R., & Mhemid, S. (2023). Sustainable production of an iron-eggshell nanocomposite and investigating its catalytic potential for phenol removal. *Ecological Chemistry and Engineering S*, *30*(3), 0–3. https://doi.org/10.2478/eces-2023-0040

31. Mustafa, Y. A., & Shihab, A. H. (2013). Removal of 4-chlorophenol from wastewater using a pilot-scale advanced oxidation process. *Desalination and Water Treatment*, *51*(34–36), 6663–6675. https://doi.org/10.1080/19443994.2013.765362

32. Olu-Owolabi, B. I., Alabi, A. H., Diagboya, P. N., Unuabonah, E. I., & Düring, R. A. (2017). Adsorptive

removal of 2,4,6-trichlorophenol in aqueous solution using calcined kaolinite-biomass composites. *Journal of Environmental Management*, *192*, 94–99. https://doi.org/10.1016/j.jenvman.2017.01.055

33. Peng, X., Xu, F., Zhang, W., Wang, J., Zeng, C., Niu, M., & Chmielewská, E. (2014a). Magnetic Fe_3O_4/silica-xanthan gum composites for aqueous removal and recovery of Pb_2^+. *Colloids and Surfaces A: Physicochemical and Engineering Aspects*, *443*, 27–36. https://doi.org/10.1016/j.colsurfa.2013.10.062

34. Pera-Titus, M., García-Molina, V., Baños, M. A., Giménez, J., & Esplugas, S. (2004). Degradation of chlorophenols by means of advanced oxidation processes: A general review. *Applied Catalysis B: Environmental*, *47*(4), 219–256. https://doi.org/10.1016/j.apcatb.2003.09.010

35. Pérez-Portuondo, I., Serrat-díaz, M., Pérez-Silva, R. M., & Ábalos-Rodríguez, A. (2021). Phytotoxic Effects of 4-Chlorophenol and 2, 4-Dichlorophenol in the Germination of Seeds of *Phaseolus vulgaris* and *Zea mayz*. *American Journal of Plant Sciences, 12*(4). https://doi.org/10.4236/ajps.2021.124041

36. Pi, G., Li, Y., Bao, M., Mao, L., Gong, H., & Wang, Z. (2016). Novel and Environmentally Friendly Oil Spill Dispersant Based on the Synergy of Biopolymer Xanthan Gum and Silica Nanoparticles. *ACS Sustainable Chemistry & Engineering, 4*(6). https://doi.org/10.1021/acssuschemeng.6b00063

37. Raja, P., Bensimon, M., Kulik, A., Foschia, R., Laub, D., Albers, P., Renganathan, R., & Kiwi, J. (2005). Dynamics and characterization of an innovative Raschig rings-TiO_2 composite photocatalyst. *Journal of Molecular Catalysis A: Chemical*, *237*(1–2), 215–223. https://doi.org/10.1016/j.molcata.2005.04.060

38. Ren, L., Zhang, J., Li, Y., & Zhang, C. (2011). Preparation and evaluation of cattail fiber-based activated carbon for 2,4-dichlorophenol and 2,4,6-trichlorophenol removal. *Chemical Engineering Journal*, *168*(2), 553–561. https://doi.org/10.1016/j.cej.2011.01.021

39. Salam, K. K., Agarry, S. E., Arinkoola, A. O., & Shoremekun, I. O. (2015). Optimization of operating conditions affecting microbiologically influenced corrosion of mild steel exposed to crude oil environments using response surface methodology. *Biotechnology Journal International, 7*(2), 68–78. https://doi.org/10.9734/BBJ/2015/16810

40. Salim, K., Sulaiman, F. A., Alwared, A. I., & Mohammed, N. A. (2024). Removal of levofloxacin from aqueous solutions by using micro algae : optimization, isotherm, and kinetic study. *Results in Engineering*, *23*(March), 102529. https://doi.org/10.1016/j.rineng.2024.102529

41. Shafqat, U., Hussain, S., Shahzad, T., Shahid, M., & Mahmood, F. (2023). Elucidating the phytotoxicity thresholds of various biosynthesized nanoparticles on physical and biochemical attributes of cotton. *Chemical and Biological Technologies in Agriculture*, 1–16. https://doi.org/10.1186/s40538-023-00402-x

42. Shihab, M. S., Ismail, H. H., & Ibrahem, A. I. (2024). Adsorptive optimization of abamectin from aqueous solutions by immobilized *Eichhornia crassipes*. *Ecological Engineering & Environmental Technology*, *25*(10), 150–157. https://doi.org/10.12912/27197050/191412

43. Sobhanardakani, S., Jafari, A., Zandipak, R., & Meidanchi, A. (2018). Removal of heavy metal (Hg (II) and Cr (VI)) ions from aqueous solutions using Fe_2O_3/SiO_2 thin films as a novel adsorbent. *Process Safety and Environmental Protection, 120,* 348-357. https://doi.org/10.1016/j.psep.2018.10.002

44. Sulaiman, F. A., & Alwared, A. I. (2022a). Ability of response surface methodology to optimize photocatalytic degradation of amoxicillin from aqueous solutions using immobilized TiO_2/Sand. *Journal of Ecological Engineering*, *23*(5), 293–304. https://doi.org/10.12911/22998993/147318

45. Sulaiman, F. A., & Alwared, A. I. (2022b). Green synthesis of TiO_2 using *Ocimum basilicum* leaf extract and its application in photocatalytic degradation of amoxicillin residues from aqueous solution. *Desalination and Water Treatment*, *262*, 312–322. https://doi.org/10.5004/dwt.2022.28504

46. Tan, I. A. W., Ahmad, A. L., & Hameed, B. H. (2009). Adsorption isotherms, kinetics, thermodynamics and desorption studies of 2,4,6-trichlorophenol on oil palm empty fruit bunch-based activated carbon. *Journal of Hazardous Materials*, *164*(2–3), 473–482. https://doi.org/10.1016/j.jhazmat.2008.08.025

47. Xu, J., Ju, C., Sheng, J., Wang, F., Zhang, Q., Sun, G., & Sun, M. (2013). Synthesis and characterization of magnetic nanoparticles and its application in lipase immobilization. *Bulletin of the Korean Chemical Society*, *34*(8), 2408–2412. https://doi.org/10.5012/bkcs.2013.34.8.2408

48. Yagub, M. T., Sen, T. K., Afroze, S., & Ang, H. M. (2014). Dye and its removal from aqueous solution by adsorption: A review. *Advances in Colloid and Interface Science*, *209*, 172–184. https://doi.org/10.1016/j.cis.2014.04.002

49. Yang, Q., Gao, M., & Zang, W. (2017). Comparative study of 2,4,6-trichlorophenol adsorption by montmorillonites functionalized with surfactants differing in the number of head group and alkyl chain. *Colloids and Surfaces A: Physicochemical and Engineering Aspects*, *520*, 805–816. https://doi.org/10.1016/j.colsurfa.2017.02.057

50. Zada, A., Khan, M., Asim, M., Khan, Q., Habibiyangjeh, A., Dang, A., & Maqbool, M. (2021). Review on the hazardous applications and photodegradation mechanisms of chlorophenols over different photocatalysts. *Environmental Research*, *195*(January), 110742. https://doi.org/10.1016/j.envres.2021.110742